International Journal of Thermal Sciences 90 (2015) 9–23

Contents lists available at ScienceDirect

International Journal of Thermal Sciences

journal homepage: www.elsevier.com/locate/ijts

Effect of aligned and offset roughness patterns on the fluid flow and heat transfer within microchannels consist of sinusoidal structured roughness

Masoud Kharati-Koopaee*, Mohsen Zare

Department of Mechanical and Aerospace Engineering, Shiraz University of Technology, Shiraz, Iran

ARTICLE INFO

Article history:
Received 6 April 2014
Received in revised form
1 November 2014
Accepted 27 November 2014
Available online

Keywords:
Aligned
Offset
Microchannel
Friction factor
Nusselt number
Thermal performance index

ABSTRACT

This research aims at numerical study of the effect of aligned and offset roughness patterns on the fluid flow and heat transfer phenomenon within rectangular cross section microchannels containing structured sinusoidal roughness. To do this, the pressure losses, heat transfer coefficients as well as thermal performance indexes in aligned pattern are compared with corresponding offset pattern at different roughness pitches, heights and microchannel heights. In this work, the upper and lower microchannel walls involve sinusoidal roughness and other walls are assumed to be smooth. Air and water are also chosen as the working fluids. To validate the current numerical model, comparisons are also made with previous experimental, theoretical and numerical results and reasonable agreements are observed. Results show that for the air, the effect of change in the channel parameters on the heat transfer coefficient is of little significance compared to the water and the two roughness arrangements represent a same behavior. It is found that, at high roughness height or low channel height, the offset arrangement provides lower pressure loss for the considered fluids and also lower heat transfer rate for water than the aligned pattern. It is shown that for both fluids, as the roughness pitch increases, the offset pattern provides lower pressure loss than the aligned pattern. Numerical results indicate that for water, the increase in roughness pitch leads to negligible variation in the heat transfer rate in aligned configuration while different behavior is observed in offset pattern. Results exhibit that both air and water represent a same thermal performance index and the offset effect could increase the thermal performance of microchannel with the increase in roughness pitch ratio. It is also revealed that, in both roughness patterns, the decrease in constricted relative roughness leads to the increase in the thermal performance index and high thermal performance is achieved at low roughness height.

1. Introduction

The development of technology in micro scale is of particular interest to the researchers due its wide range of application in micro devices. Examples of these devices include the micro-electro-mechanical systems (MEMS), micro heat exchangers, biomedical devices, etc. In this context, the design and fabrication of microchannels, which can be viewed as a heat removal element in such devices, received more attention by researchers due to ongoing progress in the aforementioned devices. The high range of application for the microchannels in different industries motivates the researchers to analyze the heat transfer rate phenomena within these devices at different conditions. Examples of these include the investigation of different environmental conditions effects such as gravity [1] or magnetic field [2] or different working fluids such as non-Newtonian fluids [3] on the heat transfer rate. The most significant characteristic associated to the microchannels is their high surface area to volume ratio that thereby causes the adequacy of these devices in transferring the heat with rather a low flow rate.

Generally, owing to machining process during fabrication, the flow passages involve random roughnesses. Colebrook [4], Nikuradse [5], and Moody [6] were pioneers in clarifying of random roughness effect on the pressure drop for flow through channels having relative roughness lower than $e/D_h = 0.05$. However, in microchannels, due to low hydraulic diameter, the relative roughness exceeds from this value and so special attention is required on

* Corresponding author.
E-mail address: kharati@sutech.ac.ir (M. Kharati-Koopaee).

http://dx.doi.org/10.1016/j.ijthermalsci.2014.11.031
1290-0729/

the roughness effect on the fluid flow in micro scale. Kandlikar [7] and Natrajan and Christensen [8] performed some experiments to investigate the effect of roughness in micro scale channels. In their work, the roughness effects on the friction factor and also in the laminar, transitional and turbulent regimes are characterized. Some researches were also conducted to analysis theoretically and experimentally the roughness effects on the liquid and gaseous fluid flow through micro passages [9,10]. In the random roughness shape, some studies investigated the roughness effect on both fluid flow and heat transfer rate. Shen et al. [11] examined the roughness effects on the friction factor and Nusselt number experimentally. Xiong and Chung [12] carried out a numerical approach to present a new model for three-dimensional roughness effects on friction factor and heat transfer in microtubes. Li et al. [13] also studied numerically and experimentally the flow and heat transfer characteristics of liquid laminar flow in rough microtubes and the condition at which the axial conduction in the tube wall was significant.

In analysis of fluid flow or heat transfer within microchannels, some studies were carried out to model the random roughness. In these works, the random roughness within micro passages was modeled somehow by some geometrically known shapes. Examples of these include modeling of random roughness by rectangular prism elements [14], triangular, rectangular, sinusoidal and random triangular waves [15–17] or random shaped micro peaks [18]. In modeling random roughness, Valdes et al. [19] examined the effect of roughness on the laminar flow through narrow and short annular channels by modeling an equivalent smooth channel. Chen et al. [20] also characterized the topography of rough surfaces using a fractal Cantor set structure to model the laminar heat transfer in rough microchannels.

The structured roughnesses, as a significant tool to enhance the heat transfer rate, were also the subject of some researches. The advantages of this type of roughness over the random roughness are their simplicity to create and also to model numerically. The most significant features associated with this type of roughness, in comparison with random roughness, are their predictability in terms of amplitude and spatial parameters. In this type of roughness, some researches were devoted to describe how the distributions of 2-D rectangular elements [21], parallelepipedic elements [22] or three-dimensional conical peaks [23] on the smooth surfaces of a plane microchannel could affect the pressure loss and Nusselt number. In these works, it was found that the impact of roughness on pressure loss was higher than the Nusselt number. In the context of structures roughness, the need to have as high as possible performance for the microchannels motivates the researchers to examine the effect of different roughness patterns such as aligned and offset configurations on the fluid flow. For instance, Rawool et al. [24] performed a three-dimensional numerical simulation of flow through serpentine microchannels composed of rectangular, triangular and trapezoidal roughness shapes in aligned and offset patterns in the form of obstructions along the channels walls. They found that the friction factor is more for rectangular and triangular obstructions and the trapezoidal geometry provided lower friction factor. Zhang et al. [25] also conducted a numerical analysis to investigate the pressure loss and heat transfer rate within microchannels consisted of surfaces with semicircular, triangular and rectangular roughness elements in aligned configuration. They found that the flow within microchannel involving semicircular and triangular roughness elements led to higher recirculation zone that resulted in enhancement of heat transfer and higher pressure drop. Some studies revealed the importance of constricted flow parameters in analyzing of fluid flow through microchannels. Brackbill and Kandlikar [26] and Wagner and Kandlikar [27] studied the effect of saw-tooth roughness elements in aligned pattern on the friction factor using the constricted flow parameters and wall function methods. They observed that the roughness led to early transition to turbulent flow and friction factors in the laminar region are predicted with reasonable accuracy using the hydraulic diameter based on the constricted flow area. Kandlikar et al. [28] carried out an experimental study to assess the effect of saw-tooth roughness in aligned and offset patterns on the pressure drop. They found that, for these roughness patterns, the use of constricted flow diameter extended the applicability of friction factor equations in laminar flow for constricted relative roughness values up to 14%. They also showed that in turbulent regime, the aligned and offset roughness patterns led to different results.

Recently, the structured sinusoidal roughness received more attention by researchers. This is with regard to the fact that, in comparison with other structured roughness shapes studied in the literature, this roughness geometry provides lower pressure loss and higher heat transfer rate due to better alignment of channel geometry with the flow and also better mixing [29]. In this roughness type, some works were carried out to characterize the effect of roughness on friction factor and Nusslet number within different microchannel geometries experimentally [30] and numerically [29]. In these researches, the aligned roughness configuration was concerned.

The main objective of this study is to provide a better understanding of the fluid flow and heat transfer rate for laminar liquid flow through microchannels composed of structured sinusoidal roughness in aligned and offset arrangements. For this purpose, considering the air and water as the working fluids, the pressure losses, heat transfer coefficients and also thermal performance indexes for fluid flow through different microchannels in aligned pattern are compared with those of corresponding offset arrangement. The results of this research could benefit the design and also optimization of microchannels in transferring the heat in micro scale devices.

2. Problem description

In this research, in order to simulate the flow through the real microchannels, three-dimensional channels were considered. The cross section of microchannels considered in this work is rectangular and upper and lower microchannel walls contained the sinusoidal structured roughness while the left and right side walls are assumed to be smooth. Fig. 1 depicts the aligned and corresponding offset pattern microchannels. In this figure, W and H denote the microchannel width and height, respectively and L represents the microchannel length. In Fig. 1, the black arrows also represent the flow direction entering the channel.

Considering the coordinate system shown in Fig. 1, the microchannel lower wall geometries in both roughness configurations would be obtained using the following:

$$y_l(x) = e\cos^4\left(\frac{\pi}{\lambda}x\right) \tag{1}$$

where e and λ represent roughness height and pitch, respectively. In aligned and offset patterns, the upper wall geometries are obtained using equations (2) and (3), respectively.

$$y_{u,\text{aligned}}(x) = H - e\cos^4\left(\frac{\pi}{\lambda}x\right) \tag{2}$$

$$y_{u,\text{offset}}(x) = H - e\sin^4\left(\frac{\pi}{\lambda}x\right) \tag{3}$$

For more illustration, the microchannel lower and upper wall shapes as well as the roughness height, pitch and microchannel

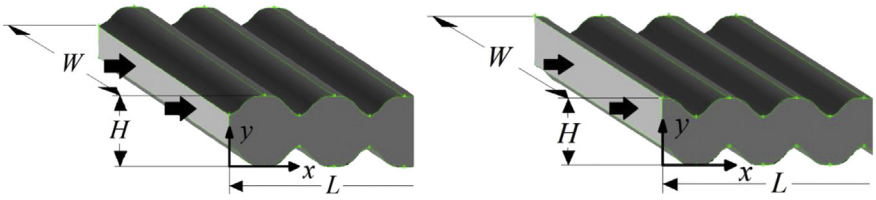

Fig. 1. The aligned (left) and corresponding offset (right) patterns.

height in aligned and corresponding offset patterns are shown in Fig. 2. This figure is provided for roughness height and pitch of $e = 70$ μm and $\lambda = 250$ μm, respectively and microchannel height of $H = 250$ μm. In this figure, H_c also represents the constricted microchannel height. As one could see, for aligned and corresponding offset roughness configurations, the roughness height, pitch, microchannel height and also the constricted microchannel height values are the same.

As presented in Fig. 2, the constricted microchannel height would be:

$$H_c = H - 2e \tag{4}$$

In order to compare the fluid flow between the aligned and offset configurations, the area-weighted average values of pressure for the two roughness patterns at the two different microchannel cross sections, spacing at the distance of Δx in the developed flow region, are extracted from the converged solution of Fluent software. Then, using the pressure difference at these cross sections over the microchannel length increment (i.e. $\Delta p/\Delta x$), the pressure losses correspond to the two different configurations are compared.

In order to compare the heat transfer rate between the aligned and offset patterns, the local heat transfer coefficients of the two roughness patterns at the thermally developed region are concerned. In the present work, the microchannel upper and lower walls are subjected to a constant heat flux while the other side walls are assumed to be adiabatic. The heat transfer coefficient at each longitudinal position, x, for both roughness configurations could be calculated as the following:

$$h = \frac{q}{\overline{T}_w - \overline{T}_f} \tag{5}$$

where q represents the heat flux and $\overline{T}_w$ and $\overline{T}_f$ represent the average heated walls and fluid temperatures, respectively, at the concerned longitudinal position, x.

Dharaiya and Kandlikar [31] showed that for rectangular cross section channels, the maximum wall temperatures were observed at the channel corners. They also stated that, at each longitudinal coordinate x, averaging the wall temperature based on the five-nodes methods along the channel width had been a good approximation for presenting the average wall temperature. Thus, at each longitudinal coordinate x, defining the microchannel upper or lower wall temperatures at five equally spaced points along the channel width as T_1, T_2, T_3, T_4 and T_5, the average upper or lower wall temperature at each longitudinal position x for both patterns would be obtained as the following:

$$\overline{T} = \frac{\left[\frac{1}{2}T_1 + T_2 + T_3 + T_4 + \frac{1}{2}T_5\right]}{4} \tag{6}$$

where T_1 and T_5 represent the wall temperatures at corners.

Having calculated the average upper or lower wall temperature at each longitudinal position x, the temperature variations for each channel wall along the channel length for the two roughness arrangements could be obtained. Finally, at each longitudinal coordinate x, the wall mean temperature could be used as representative for the average heated walls temperature (i.e. $\overline{T}_w$) and is used in equation (5) for calculation of heat transfer coefficient.

For more illustration regarding the channel walls temperature variations along the channel length, the average upper and lower wall temperatures as well as wall mean temperature verses channel length for water in the thermally developed region for aligned and corresponding offset patterns that are obtained from current work are plotted in Fig. 3. In this figure, the roughness height, pitch and channel height are $e = 100$, $\lambda = 250$ and $H = 400$ μm, respectively. In Fig. 3, the maximum and minimum wall temperatures correspond to the base and tip of the roughness elements, respectively.

The average fluid temperature is obtained from simple energy balance applied along the microchannel length, i.e.

$$\overline{T}_f = \frac{q\,l}{\dot{m}c_p} + T_i \tag{7}$$

In this equation, l and c_p represent the heated wall length along the microchannel length and specific heat, respectively, and T_i stands for the fluid temperature entering the microchannel. In equation (7), the mass flow rate through channel is also denoted as $\dot{m}$.

For smooth channels, the channel area, wetted perimeter, hydraulic diameter and Reynolds number are defined as:

$$A = HW,\quad P = 2(H + W),\quad D_h = \frac{4A}{P} \tag{8}$$

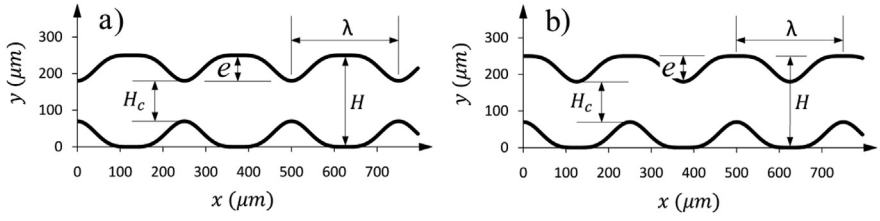

Fig. 2. Microchannel lower and upper walls, a) aligned pattern, b) offset pattern.

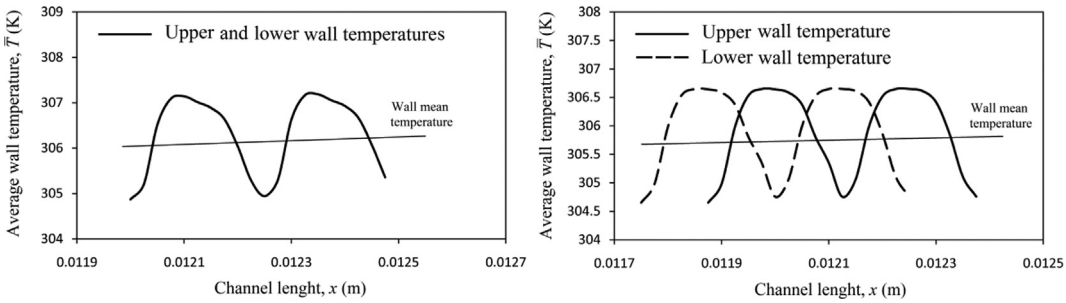

Fig. 3. Average upper and lower wall temperatures variations as well as wall mean temperature along the channel length for water in aligned (left) and offset (right) patterns.

$$\mathrm{Re} = \frac{4\dot{m}}{\mu P} \tag{9}$$

Defining the constricted microchannel height, as presented in equation (4), the constricted area, wetted perimeter, hydraulic diameter and Reynolds number for both aligned and offset patterns could be written as:

$$A_c = H_c W, \quad P_c = 2(H_c + W), \quad D_{h,c} = \frac{4A_c}{P_c} \tag{10}$$

$$\mathrm{Re}_c = \frac{4\dot{m}}{\mu P_c} \tag{11}$$

The constricted parameters are generally used in characterizing the fluid flows and heat transfer phenomenon within microchannels consisting of rough walls [29]. In microchannels, the constricted friction factor and Nusselt number are defined based on the smooth channel equations if the constricted flow parameters are used [29]. The friction factor and Nusselt number for smooth channels are as the following:

$$f = \frac{1}{2}\frac{\rho A^2 D_h}{\dot{m}^2}\frac{\Delta p}{\Delta x}, \quad \mathrm{Nu} = \frac{hD_h}{k} \tag{12}$$

So, having calculated the pressure loss and heat transfer coefficient at the developed flow region in rough channels, the constricted friction factor and Nusselt number for roughness configurations could be written as:

$$f_c = \frac{1}{2}\frac{\rho A_c^2 D_{h,c}}{\dot{m}^2}\frac{\Delta p}{\Delta x}, \quad \mathrm{Nu}_c = \frac{hD_{h,c}}{k} \tag{13}$$

In these equations, ρ, p, h and k represent the density, pressure, heat transfer coefficient and fluid thermal conductivity, respectively.

In the current work, for better understanding of fluid flow and heat transfer in the two arrangements, different microchannels with varying roughness height, pitch and microchannel height are considered. Table 1 represents the different microchannels used in the present research.

Referring to the numerical work presented by Dharaiya and Kandlikar [29], one could realize that in the considered roughness geometries and microchannel heights, the channel length of $L = 12.5$ mm would be appropriate to achieve a thermally developed region for water at the channel exit. Thus, due to lower Prandtl number of air, one could conclude that this channel length also results in a fully develop condition for air at the channel exit. So, this length is chosen as the microchannel length. In this research, in order to do the validation, the microchannel width is also considered to be $W = 12.7$ mm.

3. Numerical procedure

In this study, a three-dimensional analysis is performed and the fluid flow and heat transfer within microchannel in aligned pattern are compared with those of corresponding offset pattern using the commercial software, Fluent. The considered working fluids are air and water and enter the microchannel at the temperature of $T = 300$ K. Fluids properties are also assumed to be constant and are evaluated at the fluids inlet temperature. Assuming continuum approximation, the general form of continuity, momentum and energy equations in macroscale can be used for numerical simulations. In the considered microchannels, the velocity at the inlet and pressure at the outlet are set as the channel boundary conditions. The microchannel upper and lower walls are also subjected to a constant heat flux while the side walls are assumed to be adiabatic. Since the imposed heat flux does not affect the value of heat transfer coefficient or Nusselt number in the thermally fully developed region, the wall heat flux for air and water are chosen to be the arbitrary values of $q = 190$ W/m^2 and 19,000 W/m^2, respectively. Lin and Kandlikar [32] showed that in the case of negligible microchannel wall thickness, the axial conduction through the channel wall is of little significance. Thus, since no channel wall thickness is considered in the current work, the conduction effect through the walls is also ignored.

To analyze the fluid flow and heat transfer within the microchannels, the constricted Reynolds number for each microchannel at both roughness patterns are assumed to be $\mathrm{Re}_c = 100$. Thus, the fluid flow through channel would be laminar. Exploring literature reveals that at this flow condition, the first order upwind scheme for discretization of governing equations has adequate accuracy in analysis of fluid flow and heat transfer within microchannels [29]. So, this scheme along with the SIMPLE algorithm for the velocity–pressure coupling is utilized to perform the numerical analysis.

Table 1
The roughness and microchannel geometries used for numerical analysis.

e (μm)	λ (μm)	H (μm)
Varying roughness height		
10	250	250
30	250	250
50	250	250
70	250	250
100	250	250
Varying roughness pitch		
100	150	250
100	250	250
100	350	250
Varying channel height		
100	250	250
100	250	400
100	250	550

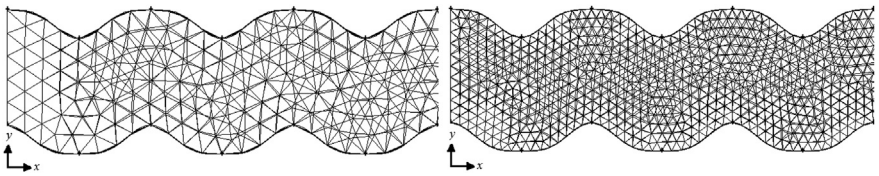

Fig. 4. Nearfield pictures of grid at which each roughness involves 9 (left) and 17 (right) nodes.

Table 2
The grid independency study for the pressure loss (N/m^3) and heat transfer coefficient (W/m^2 k) for air and water at different roughness patterns when roughness height, pitch and channel height are $e = 100$ μm, $\lambda = 250$ μm and $H = 250$ μm, respectively.

Node number	Air				Water			
	Aligned		Offset		Aligned		Offset	
	$-\Delta p/\Delta x \times 10^{-4}$	$h \times 10^{-4}$	$-\Delta p/\Delta x \times 10^{-4}$	$h \times 10^{-4}$	$-\Delta p/\Delta x \times 10^{-4}$	$h \times 10^{-4}$	$-\Delta p/\Delta x \times 10^{-4}$	$h \times 10^{-4}$
9	68.4	0.20	35.3	0.15	163.6	4.71	84.0	3.61
11	65.3	0.14	33.6	0.12	162.1	3.25	82.5	2.93
13	64.6	0.12	32.7	0.09	161.7	2.82	81.8	2.05
15	64.5	0.11	32.7	0.08	161.6	2.55	81.6	1.97
17	64.5	0.11	32.7	0.08	161.6	2.56	81.6	1.98

The residuals are also considered as the convergence criterion and iteration is stopped when these values reach to the value of less than 10^{-6}.

4. Grid study and validation

In the present work, the microchannel geometries and corresponding grids were generated using the commercial mesh generator software, Gambit. The unstructured grid topology with Tet/Hybrid T-grid scheme is used for numerical calculations. In order to ensure the accurate computational results, a comprehensive grid independency study is performed for validating and also presenting the numerical results. To present the grid independent results, for each microchannel, the initial grid at which each roughness element contains 9 nodes is generated firstly for each roughness pattern. Thereafter, by increasing the number of nodes on each roughness to 11, 13, 15 and so on, the subsequent refined grids are obtained. Then, exploring the calculated pressure loss and heat transfer coefficient associated to these grid levels, the appropriate grid size for each microchannel at each roughness pattern would be recognized. Examination of grids indicates that for the considered working fluids, allocating of at most 17 nodes to each roughness element leads to the grid with an adequate grid resolution. Fig. 4 depicts the nearfield pictures of gird for offset configuration at which each roughness element contains 9 and 17 nodes. In this figure, the roughness height, pitch and microchannel height are $e = 50$ μm, $\lambda = 250$ μm and $H = 250$ μm, respectively.

For more illustration regarding the grid independency study, Table 2 also provides the pressure loss and heat transfer coefficient for air and water at different roughness arrangements for the case at which the roughness height, pitch and channel height are $e = 100$ μm, $\lambda = 250$ μm and $H = 250$ μm, respectively. Results show that this channel geometry corresponds to rather high flow variables gradients.

Inspecting the grids used for grid study in the all considered microchannels shows that the minimum and maximum computational cells associated with the appropriate grid sizes would be around 15 and 41 million, respectively.

To validate our current numerical models in prediction of pressure loss and heat transfer coefficient, the friction factors and Nusselt numbers obtained from present work for water are compared with those of theoretical and previously numerical and experimental works.

As presented by Kakac et al. [33], the theoretical friction factor for smooth channel could be calculated via the following:

$$f_{\mathrm{th},s} = \frac{24}{\mathrm{Re}}\left(1 - 1.3553\alpha + 1.9467\alpha^2 - 1.7012\alpha^3 + 0.9564\alpha^4 - 0.2537\alpha^5\right) \quad (14)$$

where α denoted as channel aspect ratio and is defined as:

$$\alpha = \frac{H}{W} \quad (15)$$

As mentioned earlier, Kandlikar et al. [28] showed that for constricted relative roughness values of up to $e/D_{h,c} = 0.14$, the theoretical formula presented in equation (14) could also be used for the aligned and offset configurations channels (within about 5%) if the flow parameters (i.e. the Reynolds number and channel aspect ratio) are replaced with corresponding constricted parameters. Accordingly, substituting the constricted Reynolds number and microchannel aspect ratio with the conventional ones, equation (14) is used for validation of current numerical model for friction factor. Table 3 compares the constricted friction factors obtained from current work and those of theoretical approach for the two geometrically consistent microchannels in aligned and corresponding offset patterns at constricted Reynolds number of $\mathrm{Re}_c = 100$. As one could see, there are reasonable agreements between the results.

In order to validate the current numerical model in prediction of heat transfer coefficient, the Nusselt numbers obtained from the present work for water and those of Dharaiya and Kandlikar [29] and Lin and Kandlikar [30] are compared. In these works, the flow regime was laminar and the channels had a sinusoidal

Table 3
Comparison of constricted friction factors obtained from current work for water and those of theoretical approach for aligned and offset patterns.

H (μm)	λ (μm)	e (μm)	$e/D_{h,c}$	α_c	f_{th}	$f_{\mathrm{num,aliged}}$	$f_{\mathrm{num,offset}}$	Max. error (%)
250	250	30	0.080	0.01496	0.235	0.222	0.226	5.5
550	250	100	0.146	0.02756	0.231	0.218	0.221	5.6

Table 4
Comparison of Nusselt numbers obtained from current work for water and those of numerical and experimental approaches for aligned pattern.

H (μm)	λ (μm)	e (μm)	Re	Nu (present work)	Nu	Error (%)
250	250	50	100	14.84	14.87[a]	0.2
450	250	96.3	350	18.63	20[b]	6.8

[a] Numerical result of Dharaiya and Kandlikar [29].
[b] Experimental result of Lin and Kandlikar [30].

roughness in aligned pattern. In Ref. [29], a numerical calculation at Reynolds number of Re = 100 was concerned while in Ref. [30], an experimental approach was conducted at different Reynolds numbers. Table 4 represents the channel geometries, flow conditions and also Nusselt numbers obtained from current work and those of numerical and experimental works. This table confirms that the present numerical model has adequate accuracy in predicting of Nusselt number for flow within considered microchannels in laminar flow regime.

5. Numerical results and discussion

As mentioned earlier, comparison of fluid flow and heat transfer within microchannel in the two arrangements is studied in the thermally developed flow region. In order to ensure the adequacy of considered channel length to have a thermally developed region, the channel wall temperature associated to the roughness tip and fluid temperature along the channel length for air and water are presented in Figs. 5 and 6 for the aligned and corresponding offset pattern. These figures are provided for the channel having maximum hydraulic diameter (i.e. the channel with the height of $H = 550$ μm). In these figures, the tip wall temperature is extracted from the converged solution of software and average fluid temperature is computed using equation (7). As presented in Ref. [34], in the case of constant channel wall heat flux, the thermally fully developed condition is achieved when the average channel wall or fluid temperature derivative respect to the channel length is constant (i.e. $d\overline{T}_w/dx = d\overline{T}_f/dx = qP/\dot{m}\,c_p$). Exploring these figures reveals that in the considered microchannels, the slope of variations of wall tip or fluid temperature along the channel length reaches to a constant value as the fluid moves toward the channel exit. This implies that the thermally fully developed condition is met and the considered channel length (i.e. $L = 12.5$ mm) is appropriate in order to have a thermally developed condition at the channel exit. Thus, that the thermally developed condition also occurs at the end of other channels having lower hydraulic diameter. Since the Prandtl numbers of considered working fluids are in the order of or higher than unity, the thermally fully developed condition at the channel exit ensure us to have also a hydrodynamically fully developed condition at the end of channel. Figs. 5 and 6 reveal that the thermal entrance length for air is lower than that of water due to lower Prandtl number of air. These figures also indicate that the offset effect has a little effect on the thermal entrance region.

In order to assess the fluid flow and heat transfer within microchannel in the aligned and offset configurations, the pressure losses and heat transfer coefficients and corresponding constricted friction factors and Nusselt numbers as well as thermal performance indexes in aligned pattern are compared with those of corresponding offset pattern in the developed flow region.

5.1. Effect of roughness patterns at varying roughness height

Fig. 7 represents the line plots of pressure loss and heat transfer coefficient for air and water at different roughness heights. In these figures, the roughness pitch and microchannel height are $\lambda = 250$ μm and $H = 250$ μm, respectively. This figure shows that in the considered working fluids, the offset pattern provides lower pressure loss compared to the aligned pattern and differences

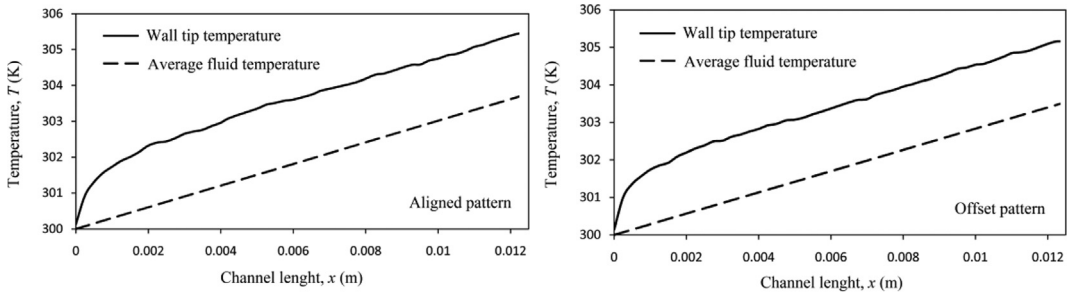

Fig. 5. Wall tip and average fluid temperatures along the channel length for water at different patterns when roughness height, pitch and channel height of $e = 100$, $\lambda = 250$ and $H = 550$ μm, respectively.

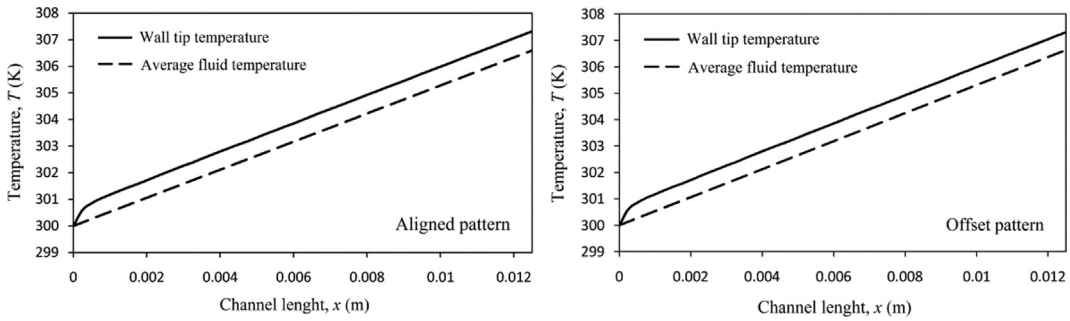

Fig. 6. Wall tip and average fluid temperatures along the channel length for air at different patterns when roughness height, pitch and channel height of $e = 100$, $\lambda = 250$ and $H = 550$ μm, respectively.

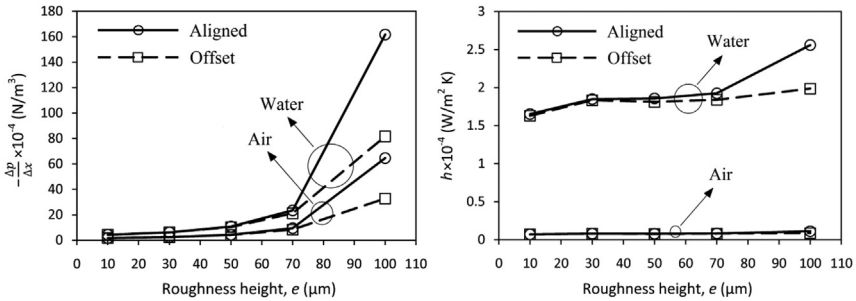

Fig. 7. Pressure loss and heat transfer coefficient for air and water at different roughness heights at roughness pitch and microchannel height of λ=250 μm and $H = 250$ μm, respectively.

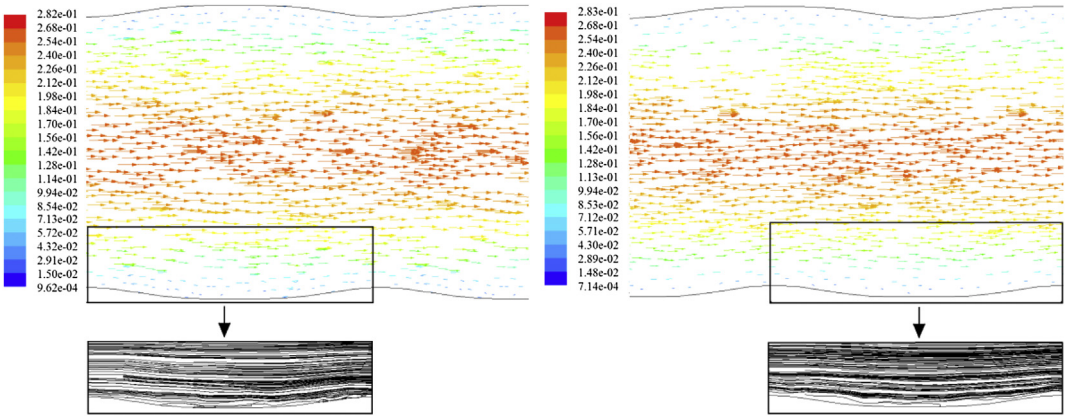

Fig. 8. Velocity vectors and streamlines within microchannel for water in aligned (left) and corresponding offset (right) patterns for roughness height of $e = 10$ μm when roughness pitch and channel height are $\lambda = 250$ μm and $H = 250$ μm, respectively.

between the two configurations is of little significance at low roughness heights. Fig. 7 shows that the effect of change in the roughness height on the heat transfer coefficient of air is of little significance compared to water and there is also a negligible difference between the two roughness patterns. This figure also represents that for water, the offset arrangement leads to lower heat transfer coefficient and discrepancies between the two patterns at high roughness height are of more significant than the low roughness height.

As presented in Fig. 7, as the roughness height increases, the pressure loss increases in both roughness configurations for the considered fluids. It could also be seen that at low values of roughness height, the differences between aligned and offset patterns in terms of the pressure loss are of little significance whereas at high values of roughness height, the pressure loss in offset pattern is lower than that of aligned pattern. To illustrate the flow structure for the considered working fluids as the roughness height increases, velocity vectors as well as streamlines within microchannels correspond to the water at different roughness heights are depicted in Figs. 8–12. Exploring these figures reveals that, in both roughness patterns, the increase in roughness height results in the increase in the fluid velocity in the channel center and also the

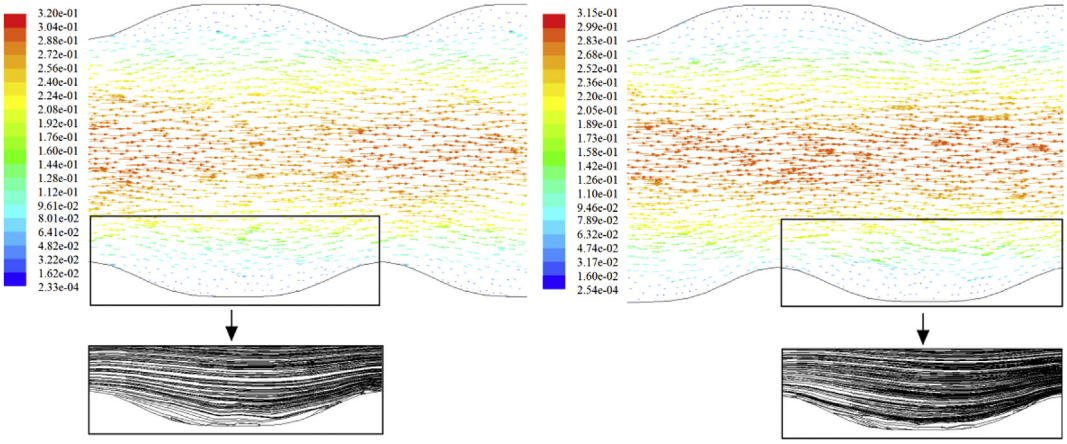

Fig. 9. Velocity vectors and streamlines within microchannel for water in aligned (left) and corresponding offset (right) patterns for roughness height of $e = 30$ μm when roughness pitch and channel height are $\lambda = 250$ μm and $H = 250$ μm, respectively.

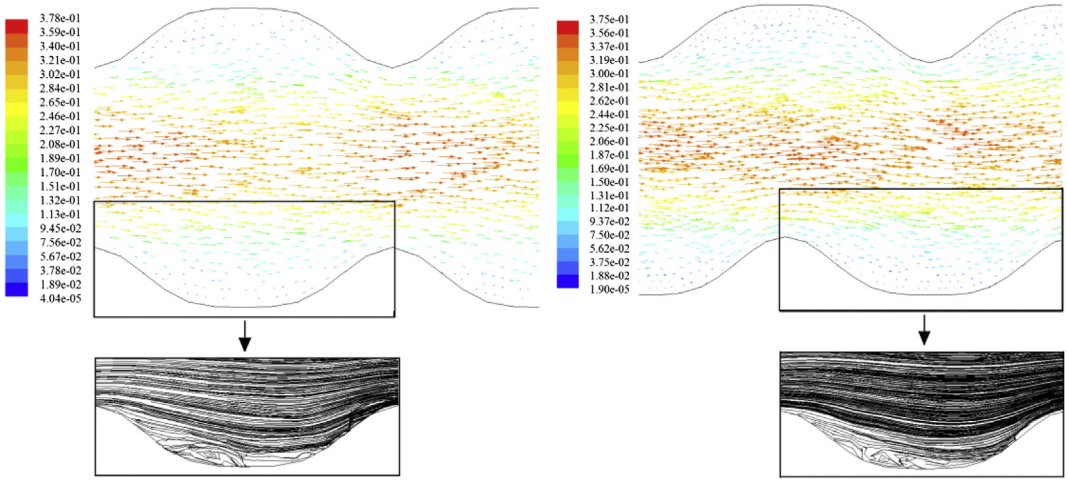

Fig. 10. Velocity vectors and streamlines within microchannel for water in aligned (left) and corresponding offset (right) patterns for roughness height of $e = 50$ μm when roughness pitch and channel height are $\lambda = 250$ μm and $H = 250$ μm, respectively.

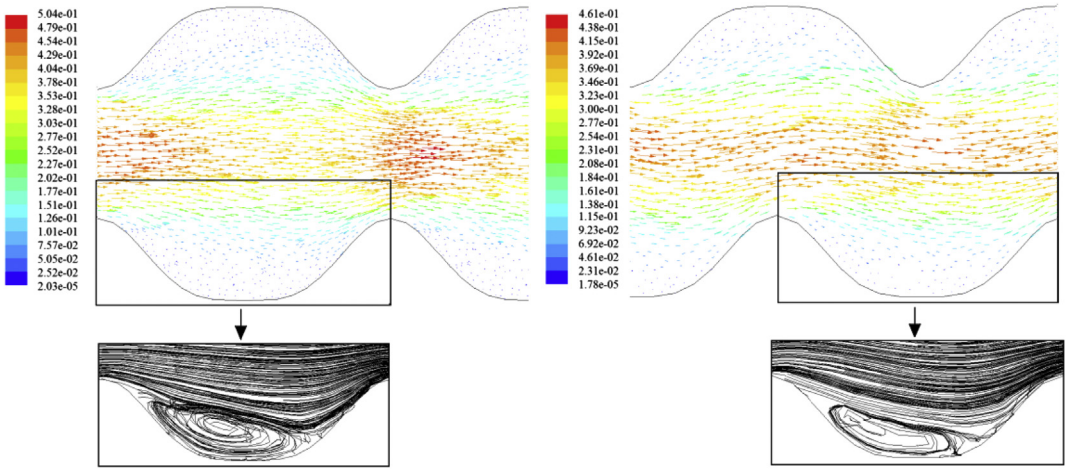

Fig. 11. Velocity vectors and streamlines within microchannel for water in aligned (left) and corresponding offset (right) patterns for roughness height of $e = 70$ μm when roughness pitch and channel height are $\lambda = 250$ μm and $H = 250$ μm, respectively.

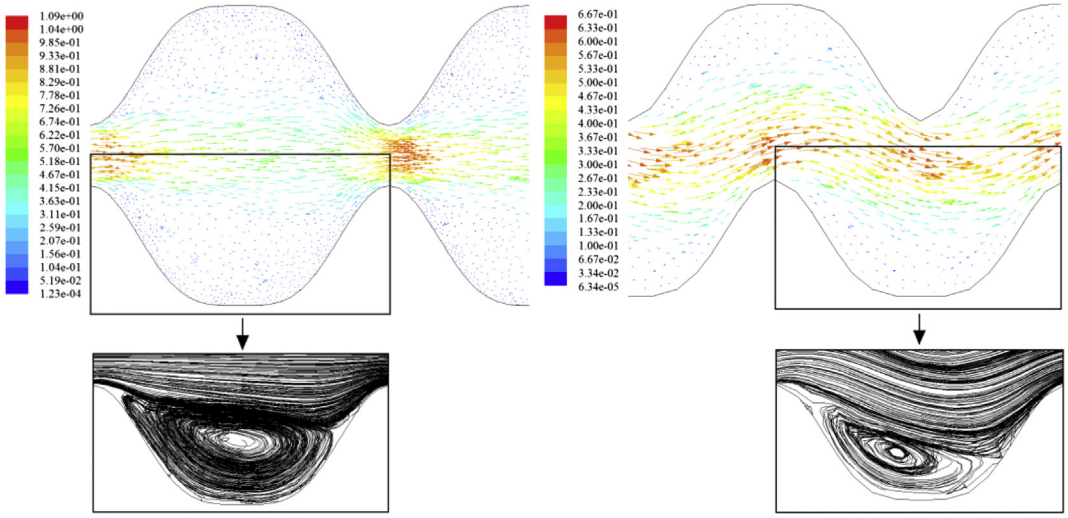

Fig. 12. Velocity vectors and streamlines within microchannel for water in aligned (left) and corresponding offset (right) patterns for roughness height of $e = 100$ μm when roughness pitch and channel height are $\lambda = 250$ μm and $H = 250$ μm, respectively.

recirculation bubble size. These effects, in turn, lead to higher pressure loss within channels in the two roughness patterns. Exploring these figures shows that, at low values of roughness height, no recirculation bubbles are formed and there are also little differences between fluid maximum velocities in the channel center in the two roughness patterns. These figures exhibit that, as the roughness height increases, the increase in the fluid maximum velocities in the channel center in offset pattern is lower than those of aligned configuration. Results also indicate that, with the increase in roughness height, the formed recirculation bubbles size in offset pattern is slightly lower than those of aligned pattern. Thus, one could easily conclude that at low values of roughness height, the pressure losses in both roughness configurations are nearly the same while at high roughness height values, the offset pattern provides lower pressure loss than of corresponding aligned configuration.

As mentioned earlier, considering the air as the working fluid, the change in the roughness height has a little effect on the heat transfer coefficient of the two roughness configurations and the two patterns also show a same behavior. However, different behaviors are observed for water. The following paragraphs in this subsection focus on the effect of roughness height in the two roughness configurations for water.

Fig. 7 shows that at low roughness height value, i.e. $e = 10$ μm, there are little discrepancies between heat transfer coefficients in both patterns. Referring to Fig. 8, one could see that at this roughness height, little differences exist between velocity magnitudes in the channel center in the two roughness arrangements. Exploring Fig. 8 also shows that at this roughness height, no recirculation zones are formed in the roughness bases of the two roughness arrangements. Thus, the key parameter in characterizing of heat transfer coefficients in both patterns would be velocity magnitude in the channel center. Accordingly, the heat transfer coefficient in the two roughness patterns is nearly the same.

Fig. 7 also indicates that at both roughness structures, as the roughness height increases from $e = 10$ to $e = 30$ μm, there would be an increase in the heat transfer coefficient. Inspecting Figs. 8 and 9, one could see that in both patterns, the increase in roughness height from $e = 10$ to $e = 30$ μm causes the channel surface area and also the maximum fluid velocity in the channel center to increase. As presented in these figures, the recirculation zone sizes in the roughness base at these roughness heights are of little importance and thus, the key parameter in characterizing of heat transfer coefficients in both patterns would also be the channel surface area as well as the fluid velocity magnitude in the channel center. Consequently, in the two configurations, the increase in roughness height from $e = 10$ to $e = 30$ μm leads to increase in heat transfer coefficient whereas the offset pattern tends to provide lower heat transfer rate than of corresponding aligned structure due to lower velocity magnitude in the channel center.

Results show that at roughness height range of $e = 30$ to $e = 70$ μm, the heat transfer coefficient variations are of less significance. Figs. 9 and 10 exhibit that, in both patterns, the increase in roughness height from $e = 30$ to $e = 50$ μm causes the recirculation zone to be formed in the roughness bases. Figs. 9–11 show that, at this roughness height range, the increase in roughness height leads to increase in the channel surface area and also the fluid velocity in the channel center and also causes the formed recirculation bubbles (that are nearly equal in size in the two patterns) to become bigger. Thus, in both roughness structures and at this roughness height range, as the roughness height increases, the favorable effect of increase in the channel surface area and also the fluid velocity in the channel center is counteracted by undesirable effect of increase in the recirculation bubble size. Thus, the heat transfer coefficient variation with roughness height in this roughness height is of less significance. Fig. 7 also indicates that at this range of roughness height, the offset pattern tends to provide lower heat transfer rate than the aligned pattern. This phenomenon could also be interpreted based on the higher velocity magnitude occurs in the channel center in the aligned pattern than the offset one.

Fig. 7 shows that the increase in the roughness height from $e = 70$ to $e = 100$ μm causes the heat transfer rate in the two patterns to increase. Referring to Fig. 12, it implies that the channel surface area and velocity of fluid in the channel center have more contribution than the recirculation bubble size in determining of heat transfer rate. Results also shows that the offset pattern provides lower heat transfer rate than the aligned pattern and difference between the two patterns is rather remarkable. Exploring Fig. 12 shows that, although the recirculation bubble size in the offset pattern is slightly lower than that of aligned pattern, however, the maximum velocity magnitude in the channel center is about 0.6 times that of the aligned configuration. Thus, in this roughness height range, the channel center velocity magnitude has more contribution than the recirculation bubble size in determining the rate of heat transfer.

5.2. Effect of roughness patterns at varying roughness pitch

Fig. 13 represents the line plots of pressure loss and heat transfer coefficient for both fluids at different roughness pitches. In these figures, the roughness height and microchannel height are $e = 100$ and $H = 250$ μm, respectively. As presented in this figure, for the two considered fluids, the offset pattern provides lower pressure loss in comparison with aligned pattern. Results reveal that for air, the change in roughness pitch has a negligible effect on the heat transfer coefficient in comparison with water and a similar behavior is observed for the two roughness arrangements. Fig. 13 also reveals that for water, the heat transfer coefficients in both patterns are nearly the same at low roughness pitch whereas at high roughness pitch, different behaviors are observed.

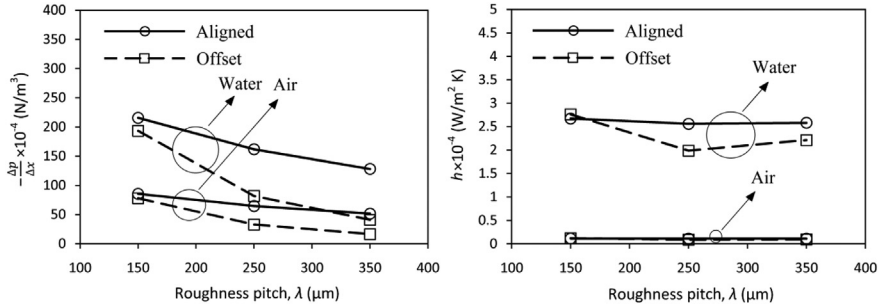

Fig. 13. Pressure loss and heat transfer coefficient for air and water at different roughness pitches at roughness height and microchannel height of $e = 100$ and $H = 250$ μm, respectively.

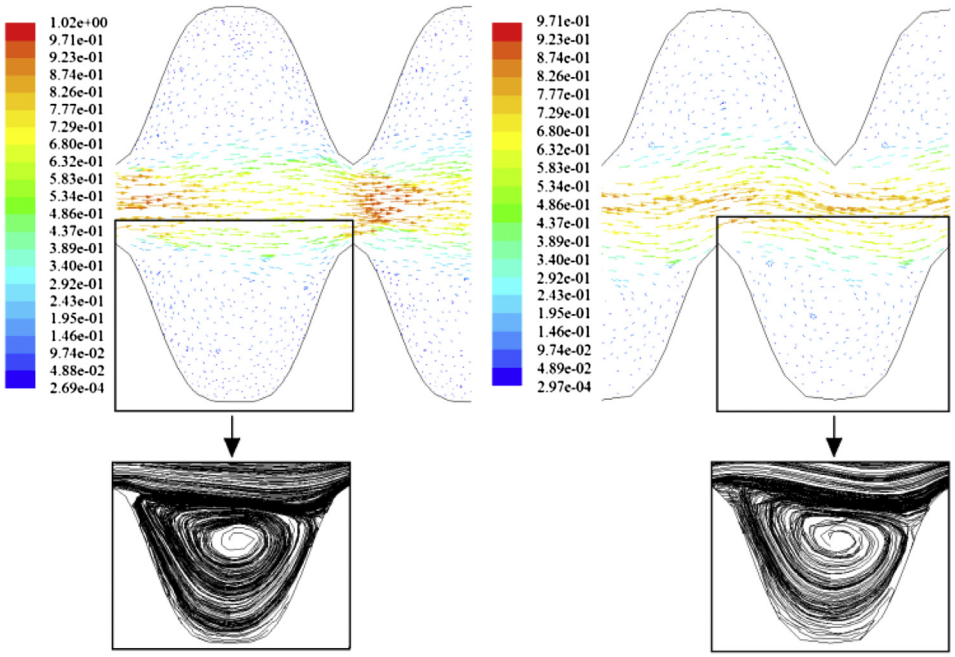

Fig. 14. Velocity vectors and streamlines within microchannel for water in aligned (left) and corresponding offset (right) patterns for roughness pitch of $\lambda = 150$ μm when roughness and channel height are $e = 100$ μm and $H = 250$ μm, respectively.

Fig. 13 shows that for air and water, an increase in roughness pitch leads to a decrease in pressure loss in both patterns. It is obvious that in both roughness patterns, an increase in roughness pitch in a constant length channel actually leads to a decrease in the number of constricted flow areas in the channel. Thus, an increase in roughness pitch results in reducing the channel wall areas at which the high shear stresses occur and leads to a decrease in pressure loss in the two arrangements. For better understanding of flow structure for the considered fluids as the roughness pitch varies, one could refer to Figs. 12, 14 and 15 that present the velocity vectors as well as streamlines for water. These figures show that an increase in roughness pitch in offset pattern causes the fluid velocity in the channel center to decrease and be lower than that of the aligned pattern. These figures also reveal that an increase in roughness pitch in offset configuration leads the recirculation bubble size to decrease. Consequently, the offset pattern results in a lower pressure loss compared to the aligned pattern.

As presented in Fig. 13, at low roughness pitch value, there is a little difference in heat transfer coefficient of water in aligned and offset patterns. Referring to Fig. 14, one could see at low roughness pitch, there are little differences between the channel center velocity magnitudes and the recirculation bubble sizes for both patterns. Thus, the offset has nearly no effect on heat transfer coefficient. Figs. 12, 14 and 15 show that for water, in aligned pattern, the increase in roughness pitch causes a negligible change in the channel center velocity magnitude and also the vertical length of recirculation bubble. Thus, as the roughness pitch increases, the change in heat transfer coefficient in aligned pattern is of little significance. However, in offset pattern, the increase in roughness pitch results in the decrease and increase in heat transfer coefficient thereafter. Comparison of Figs. 14 and 12 shows that in this roughness configuration, as the roughness pitch increases from $\lambda = 150$ to $\lambda = 250$ μm, there would be rather a little decrease in the vertical size of recirculation bubble but rather a significant decrease in the channel center velocity magnitude. This effect, in turn, causes the heat transfer coefficient to decrease. In this roughness arrangement, the increase in roughness pitch from $\lambda = 250$ to $\lambda = 350$ μm leads to a little variation in the channel

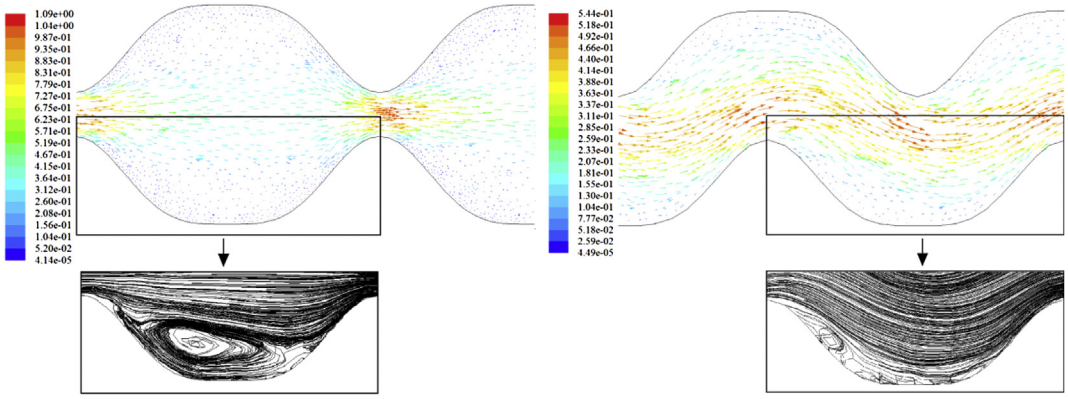

Fig. 15. Velocity vectors and streamlines within microchannel for water in aligned (left) and corresponding offset (right) patterns for roughness pitch of $\lambda = 350$ μm when roughness and channel height are $e = 100$ μm and $H = 250$ μm, respectively.

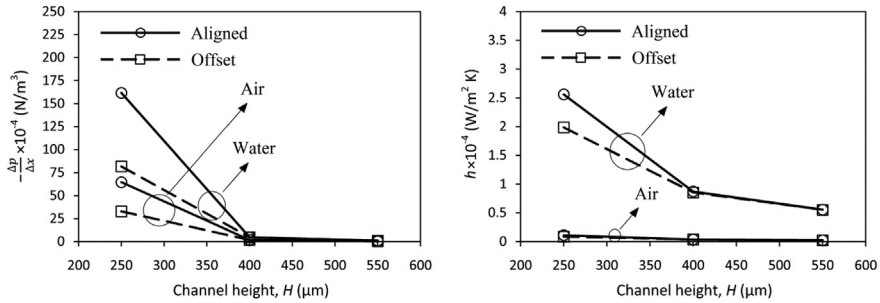

Fig. 16. Pressure loss and heat transfer coefficient for air and water at different channel heights at roughness height and pitch of $e = 100$ μm and $\lambda = 250$ μm, respectively.

center velocity but a remarkable reduction in recirculation bubble size (see Figs. 12 and 15). This phenomenon results in the increase in heat transfer coefficient.

5.3. *Effect of roughness patterns at varying channel height*

Fig. 16 represents the line plots of pressure loss and heat transfer coefficient for the considered fluids at different channel heights. This figure is provided for roughness height and pitch of $e = 100$ and $\lambda = 250$ μm, respectively. This figure indicates that for both fluids, the offset pattern provides lower pressure loss than the aligned configuration. Results also show that for air, as the channel height increases, although the trend of variation for the heat transfer coefficient of air is the same as water, however, less change is observed compared to water and the two roughness patterns represent a same behavior. Fig. 16 shows in the case of water, as the channel height increases, the offset pattern provides lower heat transfer coefficient in comparison with the aligned pattern and differences are significant at low channel heights.

The physical reasoning regarding the effect of roughness structures on the pressure loss and heat transfer coefficient at varying channel height could also be presented based on flow structure. To characterize the structure of flow for the considered fluids as the channel height increases, the velocity vector and also streamline at different channel heights that are provided for water are presented in Figs. 12, 17 and 18. These figures exhibit that in both roughness structures as the channel height increases, the fluid velocity in channel center decreases while the change in recirculation bubble size is negligible. Accordingly, the pressure loss for the two fluids and also the heat transfer coefficient of water decreases in both structures as the channel height increases. Fig. 16 exhibits that at low channel height (i.e. $H = 250$ μm), as discussed earlier, the offset effect provides lower pressure loss for the considered fluids and also lower heat transfer coefficient for water than the corresponding aligned pattern. This figure also indicates that as the channel height increases, there would be little differences in terms of pressure loss for the two fluids and also the heat transfer coefficient for water between the two patterns. As presented in Figs. 17 and 18, the increase in the channel height causes the discrepancies between the fluid velocities in the channel center in the two roughness arrangement to decrease. As stated earlier, as the channel height increase, the formed recirculation bubbles are nearly equal in size in the two patterns. Thus, the aligned and offset patterns would have an equal performance in terms of the pressure loss for air and water and also the heat transfer coefficient for water.

Figs. 7, 13 and 16 also demonstrate that at each roughness configuration, as the roughness height, pitch and channel height vary, water provides higher pressure loss and also heat transfer coefficient than the air.

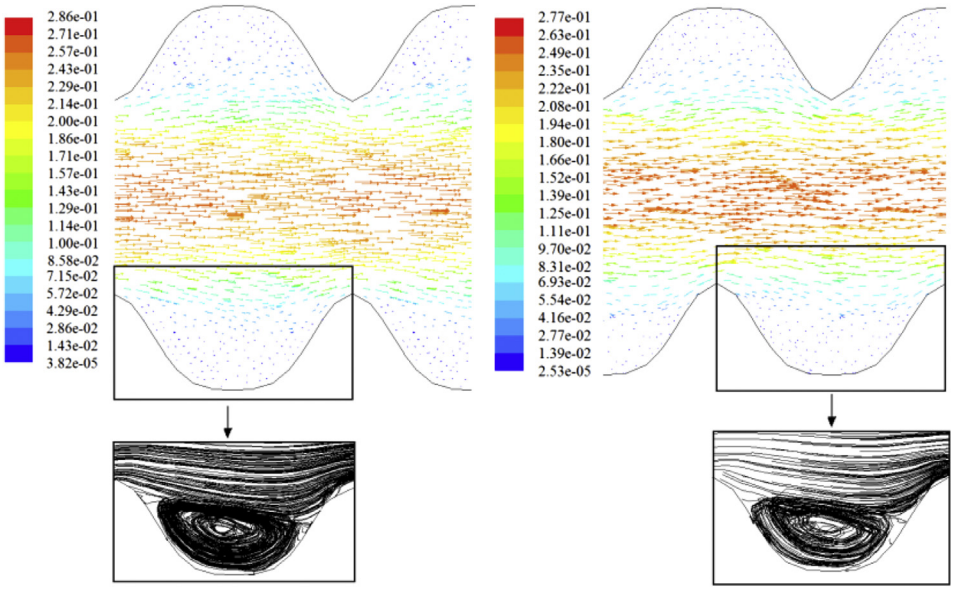

Fig. 17. Velocity vectors and streamlines within microchannel for water in aligned (left) and corresponding offset (right) patterns for channel height of $H = 400$ μm when roughness height and pitch are $e = 100$ μm and $\lambda = 250$ μm, respectively.

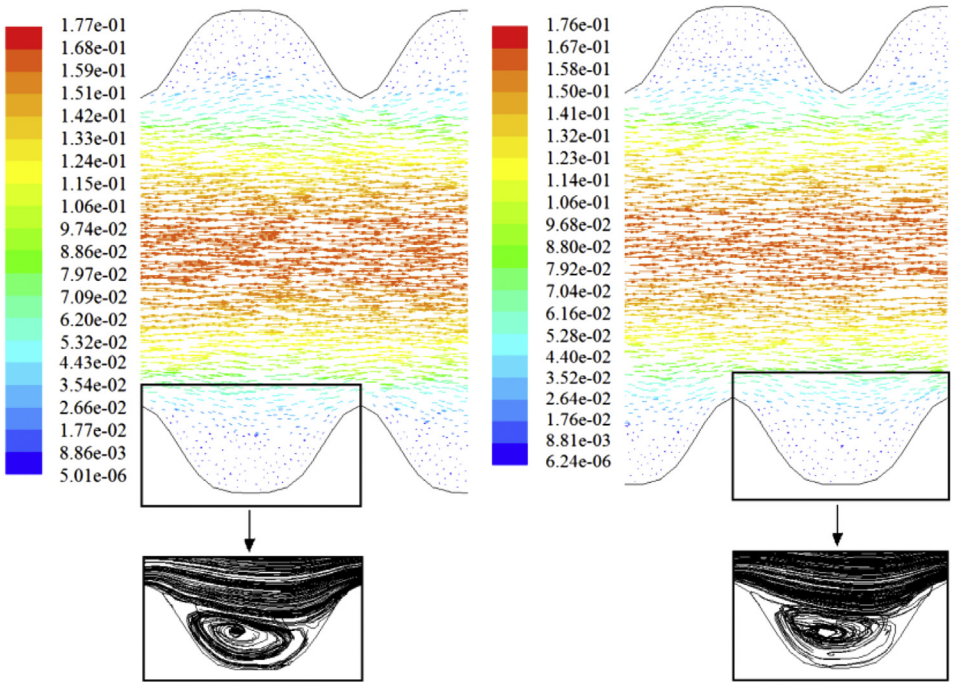

Fig. 18. Velocity vectors and streamlines within microchannel for water in aligned (left) and corresponding offset (right) patterns for channel height of $H = 550$ μm when roughness and channel height are $e = 100$ μm and $\lambda = 250$ μm, respectively.

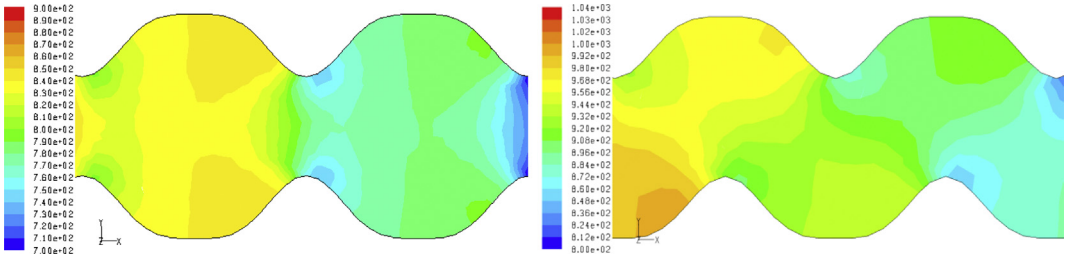

Fig. 19. Contour of pressure distribution (pa) within the channel for water at the two roughness configurations.

In order to compare the fluid pressure and temperature distributions within the microchannel at the two roughness patterns, the contour of pressure and temperature distributions for water are presented in Figs. 19 and 20. In these figures, the roughness height, pitch and channel height are $e = 70$ μm, $\lambda = 250$ μm and $H = 250$ μm, respectively. Fig. 19 exhibits that the main difference between the two arrangements is that the offset configuration leads to a smoother variation of fluid pressure at the channel center than the aligned pattern. Fig. 20 also demonstrates that the fluid temperature distribution pattern for the two arrangements is nearly the same and high temperature zone is observed at the roughness base.

Table 5 represents the constricted friction factors and Nusselt numbers associated to the considered channels for air and water. As one could see, the computed constricted friction factor and Nusselt number for air and water are nearly the same and the maximum difference is less than 2 percent. The discrepancies between friction factors and Nusselt numbers could be attributed to the computational errors. The independency of friction factor or Nusselt number value on the type of the fluid in the fully developed region of laminar flows within the rough channels is not out of mind as the other researchers also pointed it out [28,35]. This table shows that, with the increase in roughness pitch, the trend of variations in constricted friction factor and Nusselt number are similar to

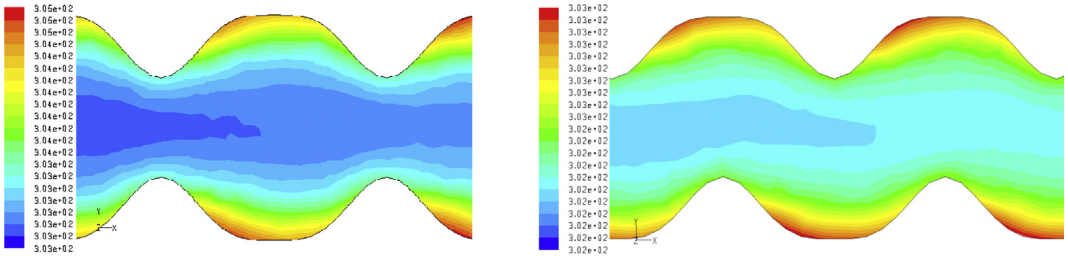

Fig. 20. Contour of temperature distribution (K) within the channel for water at the two roughness configurations.

Table 5
Constricted friction factors and Nusselt numbers for air and water for the considered microchannels.

e (μm)	λ (μm)	H (μm)	f_c (aligned)		f_c (offset)		Nu_c (aligned)		Nu_c (offset)	
			Air	Water	Air	Water	Air	Water	Air	Water
Varying roughness height										
10	250	250	0.2709	0.2704	0.2750	0.2742	12.212	12.169	11.980	12.004
30	250	250	0.2230	0.2220	0.2256	0.2261	11.352	11.285	11.356	11.194
50	250	250	0.1910	0.1906	0.1858	0.1842	8.821	8.975	8.601	8.763
70	250	250	0.1663	0.1651	0.1482	0.1495	6.821	6.847	6.587	6.542
100	250	250	0.1091	0.1092	0.0553	0.0550	4.188	4.157	3.285	3.226
Varying roughness pitch										
100	150	250	0.1436	0.1447	0.1309	0.1302	4.260	4.340	4.550	4.537
100	250	250	0.1091	0.1092	0.0553	0.0550	4.188	4.157	3.285	3.226
100	350	250	0.0870	0.0863	0.0276	0.0275	4.152	4.191	3.550	3.601
Varying channel height										
100	250	250	0.1091	0.1092	0.0553	0.0550	4.188	4.157	3.285	3.226
100	250	400	0.1937	0.1933	0.1943	0.1951	5.475	5.558	5.430	5.487
100	250	550	0.2192	0.2182	0.2220	0.2213	6.061	6.151	6.045	6.123

pressure loss and heat transfer coefficient in both roughness configurations. In this table, the cause of decrease or increase in constricted friction factors and Nusselt numbers with the increase in roughness height or channel height could be attributed to the effect of change in constricted channel area and hydraulic diameter.

5.4. Effect of roughness patterns on the thermal performance index

In the design process of microchannels, the condition at which high performance occurs (i.e., the condition at which a channel provides as low as possible friction loss along with as high as possible heat transfer rate) is an important issue. Indeed, a favorable channel is the one that provides higher heat transfer coefficient while requires minimum pumping power. Thus, in order to have a desirable channel performance, both the channel capability in transferring the heat and friction loss must be taken into account.

The preceding sections compared the pressure losses and heat transfer coefficients associated to the considered microchannels in the aligned and offset arrangements for air and water and described the situations at which high heat transfer rate may occur. However, the question may arise regarding the condition at which a microchannel may operate with as high as possible performance. As presented by Lin and Kandlikar [30], the thermal performance index, η, that compares somehow the capability of microchannel in transferring the heat to the pumping power requirement could be defined as the following:

$$\eta = \frac{\frac{\mathrm{Nu}}{\mathrm{Nu}_{\mathrm{th},s}}}{\left(\frac{f}{f_{\mathrm{th},s}}\right)^{\frac{1}{3}}} \tag{16}$$

In equation (16), f and Nu stand for friction factor and Nusselt number, respectively, for rough channels based on the channel hydraulic diameter (equation (12)). In this equation, $f_{\mathrm{th},s}$ and $\mathrm{Nu}_{\mathrm{th},s}$ also represent the corresponding theoretical friction factor and Nusselt number for smooth channels. The theoretical friction factor for smooth channel is calculated according to equation (14). The theoretical Nusselt number for smooth channel is also calculated via the following [30]:

$$\mathrm{Nu}_{\mathrm{th},s} = 8.235\left(1 - 2.0421\alpha + 3.0853\alpha^2 - 2.4765\alpha^3 + 1.0578\alpha^4 - 0.1861\alpha^5\right) \tag{17}$$

As mentioned earlier, for the fully developed laminar flow, the numerically computed friction factors and Nusselt numbers for air and water are nearly the same. Thus, based on the equation presented for the calculation of theoretical values of friction factor (equation (14)) and Nusselt number (equation (17)), the two considered working fluids represent a same thermal performance index. Figs. 21–23 represent the thermal performance index for the considered working fluids and microchannels. These figures reveal that the effect of offset on the thermal performance index is of a little significance except at varying roughness pitch. Physically, in the cases of varying roughness height or microchannel height, it could be attributed to the equal contribution of roughness in increasing or decreasing the heat transfer rate and pressure loss. As presented in Fig. 22, the increase in roughness pitch could increase the thermal performance of channel. Results show that in the considered microchannels and flow condition, the offset effect increases the thermal performance to about 25 percent. Thus, one could realize that the roughness pitch ratio, i.e. λ/e, is a significant parameter in characterizing the channel thermal performance and increase in this parameter could lead to enhancement of thermal performance index.

Fig. 21 shows that for both patterns, the increase in roughness height results in the decrease in thermal performance. Fig. 23 also indicates that the increase in channel height causes the thermal performance to increase. Calculating the constricted relative roughness, $e/D_{h,c}$, associated to the considered channels, one could see that the decrease in roughness height or the increase in channel height results in the decrease in constricted relative roughness. So,

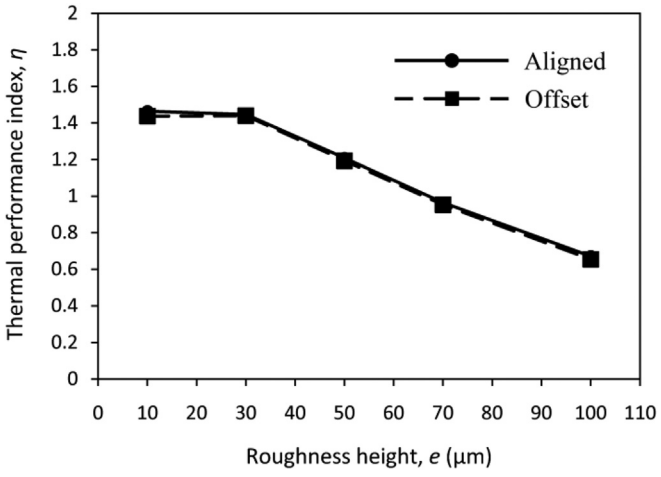

Fig. 21. Thermal performance index for air and water at different roughness height.

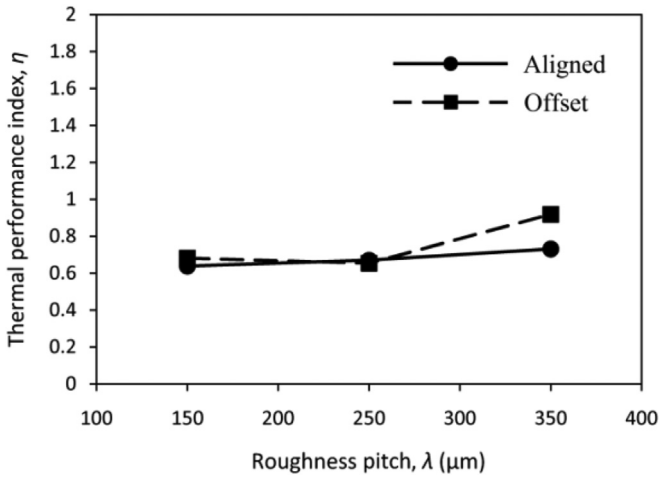

Fig. 22. Thermal performance index for air and water at different roughness pitch.

the constricted relative roughness could be viewed as an important parameter to characterize the thermal performance index of channels with varying roughness height or channel height. Thus, referring to Figs. 21 and 23, one could deduce that the decrease in constricted relative roughness leads to enhancement of thermal performance index and high thermal performance index is achievable at low roughness heights.

6. Conclusion

In the current research, for air and water as the working fluids, the effect of aligned and offset roughness patterns on the pressure drop, heat transfer rate and thermal performance index of microchannels are investigated numerically. In order to present a better understanding of the two roughness configurations roles, different microchannels with varying roughness height, pitch and channel height are considered.

It is found that the effect of change in roughness height, pitch and channel height on the heat transfer coefficient of air is of less significant than that of water and the two roughness arrangements show a similar behavior. It is found that, with the increase in roughness height, offset effect leads to lower pressure loss for air and water and also lower heat transfer rate for water than the aligned pattern and the discrepancies between the two configurations is little at low roughness heights. As the roughness pitch increase and for the considered fluids, the offset pattern provides lower pressure loss than the aligned pattern. It is also shown that for water, the effect of increase in roughness pitch causes the heat transfer rate to decrease and increase thereafter in the offset pattern while the change in roughness pitch has a negligible effect on the rate of heat transfer in the aligned pattern. Results reveals that, as the channel height decreases, the offset arrangement provides lower pressure loss for both fluids and also lower heat transfer rate for water than the aligned pattern and differences between the two roughness configurations are negligible at high channel height.

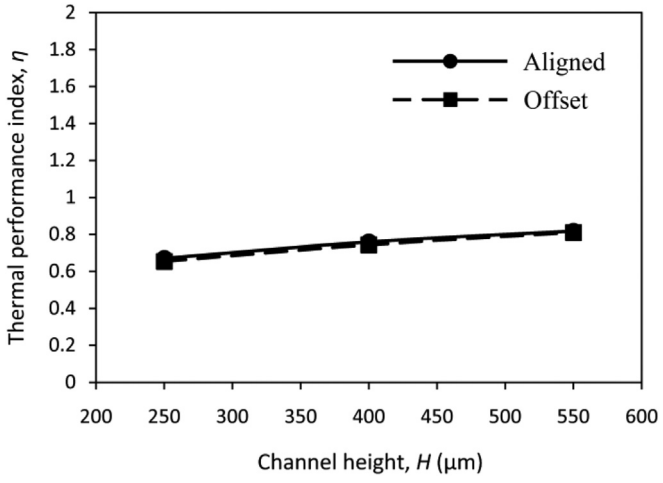

Fig. 23. Thermal performance index for air and water at different channel height.

Results indicate that the air and water results in a same thermal performance and the offset effect could increase the thermal performance index of channel with the increase in roughness pitch ratio. It is also found that, for the considered fluids and in both roughness configurations, the decrease in constricted relative roughness leads to the increase in the thermal performance index and high thermal performance index occurs at low roughness heights.

References

[1] Arash Karimipour, Alireza Hossein Nezhad, Annunziata D'Orazio, Ebrahim Shirani, Investigation of the gravity effects on the mixed convection heat transfer in a microchannel using lattice Boltzmann method, Int. J. Therm. Sci. 54 (April 2012) 142–152.
[2] A. Malvandi, D.D. Ganji, Brownian motion and thermophoresis effects on slip flow of alumina/water nanofluid inside a circular microchannel in the presence of a magnetic field, Int. J. Therm. Sci. 84 (October 2014) 196–206.
[3] Ali Esmaeilnejad, Habib Aminfarb, Mahdieh Shafiee Neistanak, Numerical investigation of forced convection heat transfer through microchannels with non-Newtonian nanofluids", Int. J. Therm. Sci. 75 (January 2014) 76–86.
[4] C.F. Colebrook, Turbulent flow in pipes with particular reference to the transition region between the smooth and rough pipe laws, J. Inst. Civ. Eng. 4 (1939) 133–156.
[5] J. Nikuradse, Laws of Flow in Rough Pipes, 1933. NACA TM No. 1292.
[6] L.F. Moody, Friction factors for pipe flow, Trans. ASME 66 (1944) 671–684.
[7] S.G. Kandlikar, Roughness effects at microscale – reassessing Nikuradse's experiments on liquid flow in rough tubes, Bull. Pol. Acad. Sci. Tech. Sci. 53 (4) (2005) 343–349.
[8] V.K. Natrajan, K.T. Christensen, The impact of surface roughness on flow through a rectangular microchannel from the laminar to turbulent regimes", Microfluid. Nanofluidics 9 (2010) 95–121.
[9] J. Zou, X.F. Peng, Effect of roughness on liquid flow behavior in ducts, in: Proceedings of FEDSM2006, ASME Joint U.S. – European Fluids Engineering Summer Meeting,, Miami, FL, July 2006.
[10] G.H. Tang, Z. Li, Y.L. He, W.Q. Tao, Experimental study of compressibility, roughness and rarefaction influences on microchannel flow, Int. J. Heat Mass Transf. 50 (2007) 2282–2295.
[11] S. Shen, J.L. Xu, J.J. Zhou, Y. Chen, Flow and heat transfer in microchannels with rough wall surface, Energy Convers. Manag. 47 (2006) 1311–1325.
[12] R. Xiong, J.N. Chung, A new model for three-dimensional random roughness effect on friction factor and heat transfer in microtubes, Int. J. Heat Mass Transf. 53 (2010) 3284–3291.
[13] Z. Li, Y.L. He, G.H. Tang, W.Q. Tao, Experimental and numerical studies of liquid flow and heat transfer in microtubes, Int. J. Heat Mass Transf. 50 (2007) 3447–3460.
[14] Y. Hu, C. Werner, D. Li, Influence of three-dimensional roughness on pressure-driven flow through microchannels, J. Fluids Eng. 125 (2003) 871–879.
[15] B.Y. Cao, M. Chen, Z.Y. Guo, Effect of surface roughness on gas flow in microchannels by molecular dynamics simulation, Int. J. Eng. Sci. 44 (2006) 927–937.
[16] G. Croce, P. D'Agaro, Numerical analysis of roughness effect on microtube heat transfer, Superlattices Microstruct. 35 (2004) 601–616.
[17] G. Croce, P. D'Agaro, Numerical simulation of roughness effect on microchannel heat transfer and pressure drop in laminar flow, J. Phys. D Appl. Phys. 38 (10) (2005) 1518–1530.
[18] M.H. Khadem, M. Shams, S. Hossainpour, Numerical simulation of roughness effects on flow and heat transfer in microchannels at slip flow regime, Int. Commun. Heat Mass Transf. 36 (2009) 69–77.
[19] J.R. Valdes, M.J. Miana, J.L. Pelegay, J.L. Nunez, T. Putz, Numerical investigation of the influence of roughness on the laminar incompressible fluid flow through annular microchannels, Int. J. Heat Mass Transf. 50 (2007) 1865–1878.

[20] Y. Chen, P. Fu, C. Zhang, M. Shi, Numerical simulation of laminar heat transfer in microchannels with rough surfaces characterized by fractal Cantor structures, Int. J. Heat Fluid Flow 31 (2010) 622–629.
[21] Y. Ji, K. Yuan, J.N. Chung, Numerical simulation of wall roughness on gaseous flow and heat transfer in a microchannel, Int. J. Heat Mass Transf. 49 (2006) 1329–1339.
[22] G. Gamrat, M.F. Marinet, S.L. Person, Modelling of roughness effects on heat transfer in thermally fully-developed laminar flows through microchannels, Int. J. Therm. Sci. 48 (2009) 2203–2214.
[23] G. Croce, P. D'agaro, C. Nonino, Three-dimensional roughness effect on microchannel heat transfer and pressure drop, Int. J. Heat Mass Transf. 50 (2007) 5249–5259.
[24] A.S. Rawool, S.K. Mitra, S.G. Kandlikar, Numerical simulation of flow through microchannels with designed roughness, Microfluid. Nanofluidics 2 (3) (2006) 215–221.
[25] C. Zhang, Y. Chen, M. Shi, Effects of roughness elements on laminar flow and heat transfer in microchannels, Chem. Eng. Process. 49 (2010) 1188–1192.
[26] T.P. Brackbill, S.G. Kandlikar, Effect of triangular roughness elements on pressure drop and laminar turbulent transition in microchannels and minichannels, in: Fourth International Conference on Nanochannels, Microchannels and Minichannels, Limerick, Ireland, June 2006.
[27] R.N. Wagner, S.G. Kandlikar, Mathematical model for fluid flow in artificially roughened microchannels, in: Proceedings of the ASME 2009 International Mechanical Engineering Congress & Exposition, Lake Buena Vista, Florida, November 2009.
[28] S.G. Kandlikar, D.J. Schmitt, A.L. Carrano, J.B. Taylor, Characterization of surface roughness effects on pressure drop in single-phase flow in minichannels, Phys. Fluids 17 (10) (2005) 100606.
[29] V.V. Dharaiya, S.G. Kandlikar, A numerical study on the effects of 2d structured sinusoidal elements on fluid flow and heat transfer at microscale, Int. J. Heat Mass Transf. 57 (2013) 190–201.
[30] T.Y. Lin, S.G. Kandlikar, An experimental investigation of structured roughness effect on heat transfer during single-phase liquid flow at microscale, ASME J. Heat Transf. 134 (10) (2012) 101701.
[31] V.V. Dharaiya, S.G. Kandlikar, Numerical investigation of heat transfer in rectangular microchannels under H_2 boundary condition during developing and fully developed Laminar flow, ASME J. Heat Transf. 134 (2) (2012) 020911.
[32] T.-Y. Lin, S.G. Kandlikar, A theoretical model for axial heat conduction effects during single-phase flow in microchannels, ASME Trans. J. Heat. Transf. 134 (2) (2012) 020902.
[33] S. Kakac, R.K. Shah, W. Aung, Handbook of Single-phase Convective Heat Transfer, John Wiley and Sons, New York, 1987.
[34] F.P. Incropera, D.P. Dewitt, Fundamentals of Heat and Mass Transfer, third ed., John Wiley & Sons, 1990.
[35] Ting-Yu Lin, Chia-Wei Chen, Chien-Yuh Yang, Satish G. Kandlikar, An experimental investigation on friction characteristics of air flow in microtube with structured surface roughness, in: 3rd Micro and Nano Flows Conference, Thessaloniki, Greece, 22–24 August, 2011.